Journal of Alloys and Compounds 835 (2020) 155325

Contents lists available at ScienceDirect

Journal of Alloys and Compounds

journal homepage: http://www.elsevier.com/locate/jalcom

Magnetism and magnetocrystalline anisotropy of tetragonally distorted $L1_0$-FeNi: N alloy

Priti Rani [a], Manish K. Kashyap [a, *], Renu Singla [a], Jyoti Thakur [b], Ali H. Reshak [c, d, e]

[a] Department of Physics, Kurukshetra University, Kurukshetra, 136119, Haryana, India
[b] Department of Physics, Guru Jambheshwar University of Science & Technology, Hisar, 125001, Haryana, India
[c] Physics Department, College of Science, Basrah University, Basrah, Iraq
[d] Department of Instrumentation and Control Engineering, Faculty of Mechanical Engineering, CTU in Prague, Technicka 4, Prague, 6 166 07, Czech Republic
[e] Nanotechnology and Catalysis Research Center (NANOCAT), University of Malaya, Kuala Lumpur, 50603, Malaysia

ARTICLE INFO

Article history:
Received 6 January 2020
Received in revised form
25 March 2020
Accepted 21 April 2020
Available online 28 April 2020

Keywords:
Permanent magnets
DFT
Magnetization
MCA
FPLAPW
SOC

ABSTRACT

We report the tunable magnetic properties of $L1_0$-FeNi via inducing tetragonal distortion with interstitial doping. For this, we have performed full potential calculations of $L1_0$-FeNi with interstitial N-doping within generalized gradient approximation. Two types of interstitial N-doping in Ni/Fe-layer of the parent alloy have been investigated. The calculated formation energy reveals the increased structure stability of tetragonally distorted FeNi via N-doping. Our calculations predict that this structural distortion induces large magnetocrystalline anisotropy at the cost of small degradation in the saturation magnetization. The increment in magnetocrystalline anisotropy is more for N-doping in Ni-layer as compared to that in Fe-layer. Hence, $L1_0$-FeNi:N alloy with N addition to Ni-layer has all the qualities to be emerged out as a probable material for permanent magnets in coming years.

1. Introduction

In modern technological society, the search for new permanent magnetic materials with specific combinations of properties (large magnetization (M_s), Curie temperature (T_C) and magnetocrystalline anisotropy (MCA)), has become intense in recent years. This combination is commonly found in rare earth (RE) - transition metal (TM) alloys, such as Nd-Fe-B and Sm–Co. However, due to the RE crisis, researchers triggered to replace RE based permanent magnetic materials with reduced RE or RE free based ones [1–5]. The main challenge in this context is to obtain a sufficiently large MCA in TM compounds. Among the possible materials for replacing RE elements in permanent magnets (PMs), the ordered $L1_0$-FeNi is the one which has large theoretically possible maximum energy product, $(BH)_{max}$ ~ 446 kJ/m^3, large saturation magnetization ~ 1.5 T, high Curie temperature ~ 830 K. Further, various researchers observed the MCA of ordered $L1_0$-FeNi oscillating around 1.0 MJ/m^3 [6–10].

Some researchers proved that the strain engineering or alloying can be used to carefully tune the properties of magnetic materials to obtain desirable functionality. Using first principles calculations, Miuara et al. [11] investigated the change in MCA of $L1_0$-FeNi with in-plane lattice parameter (a) by relaxing the perpendicular lattice parameter (c). They found that the MCA increases with decreasing a (with increasing c), reaching to a maximum value of 1.6 MJ/m^3 at a = 2.250 Å (c/a = 1.756). Indeed, Mizuguchi et al. [7] experimentally found the increase in MCA of $L1_0$-FeNi with increasing axial ratio c/a. Kojima et al. [12] examined the addition of Co in place of Fe or Ni or both in $L1_0$-FeNi films and demonstrated the slight enhancement in MCA when it is added to Ni layer only. Manchanda et al. [13] studied the $L1_0$-FeNi alloys with different doping compositions of Al, Co, Cr, Mn, Ni, P, S, Ti, V and B at substitutional/interstitial site. Out of all, they found B-atom located in the Ni-plane interstices enhances the anisotropy energy from 0.20 meV to 0.89 meV per unit cell. In order to promote the formation of $L1_0$-FeNi crystal structure, Lewis et al. [14] invented FeNi alloys doped with one or more doping elements. They found the phase stability of FeNi increases with both substitutional (Ti, V, Al) and interstitial (B and C) additions. Takata et al. [15] reported that the epitaxial films of FeNiN can be grown using the reactive molecular beam

* Corresponding author.
E-mail addresses: manishdft@gmail.com, mkumar@kuk.ac.in (M.K. Kashyap).

https://doi.org/10.1016/j.jallcom.2020.155325
0925-8388/

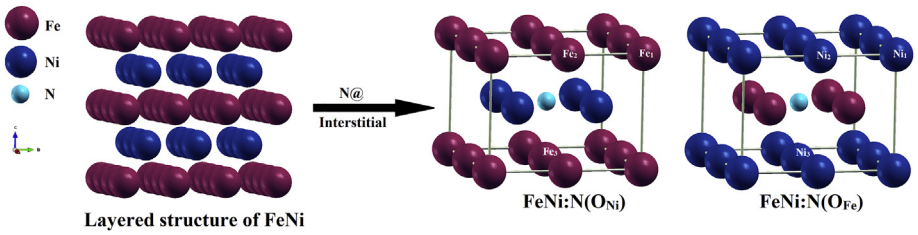

Fig. 1. Schematics of the 2 × 2 × 1 supercell of FeNi with two different kind of N-doping. FeNi:N(O_{Ni})/FeNi:N(O_{Fe}) represents N doping at interstitial sites in Ni/Fe-layer.

Table 1
Optimized lattice parameters using VASP and formation energy (E_{For}) using WIEN2k of FeNi and FeNi:N.

Alloy	Lattice Parameters		c/a	E_{For} (eV)
	a (Å)	c (Å)		
FeNi	2.531	3.579	1.414	−0.18
FeNi:N(O_{Ni})	2.561	3.714	1.450	−2.35
FeNi:N(O_{Fe})	2.554	3.778	1.479	−2.26

epitaxy technique. Goto et al. [16,17] synthesized single-phase $L1_0$-FeNi powder with a high degree of order using nitrogen insertion and topotactic extraction method. They showed that M−T curves of FeNiN show a cusp associated with the antiferromagnetic phase transition at $T_N \approx 178$ K, and positive Weiss temperature ($\theta_p \approx 100$ K). Wysocki et al. [18] investigated a route to introduce and control tetragonality in $FeNi_{1-x}Co_x$ alloys obtained by doping the $L1_0$ phase of FeNi with Co. They found that the ordered $FeNi_{0.5}Co_{0.5}$ alloy exhibits MCA as 180 μeV/atom which is larger by a factor of 4.5 from that of $L1_0$ FeNi (40 μeV/atom) .

The MCA value of $L1_0$-FeNi is insufficient for permanent magnets. In our previous study, we reported the significant effect of substitutional doping of Pt on MCA of $L1_0$-FeNi [19]. However, Pt-doping is not cost effective and cannot yield magnets at a relatively lower price. In order to maintain economical prospective, this time, we have planned to tune the MCA of $L1_0$-FeNi by a small and abundant element (N). The simulations for the same have been performed using first principles approach within the framework of density functional theory (DFT). The other aim of the present work is to check the effect of interstitial N-doping on the magnetic response of $L1_0$-FeNi.

2. Theoretical approach

$L1_0$-FeNi exists in tetragonal structure containing alternating Fe and Ni layers along the c-axis and having lattice parameters, a = 2.53 Å and c = 3.58 Å [20] (space group: *P*4/mmm). On N-doping, the lattice relaxation and movement of all the atoms were allowed to obtain the optimized structure using Vienna *ab-initio* simulation package (VASP) [21] within generalized gradient approximation (GGA). The electronic and magnetic properties of both pristine and N-doped FeNi were carried out using full potential linearized augmented plane wave (FPLAPW) method as implemented in WIEN2k [22]. For the exchange-correlation energy, we adopted the spin-polarized GGA proposed by Perdew, Becke and Ernzerhof (PBE) [23]. In FPLAPW calculations, the core states were treated fully relativistically, whereas for the valence states, a scalar relativistic approach was used. Additionally, valence electronic wavefunctions inside the Muffin-tin sphere were expanded up to $l_{max} = 10$. The radii of the Muffin-tin sphere (R_{MT}) for various atoms were taken in such a way to ensure nearly touching spheres and thus to avoid the possibility of charge leakage. The plane wave cut-off parameters were decided by $R_{MT}k_{max} = 7$ (where k_{max} is the largest wave vector of the basis set) and $G_{max} = 12$ a.u.$^{-1}$ for Fourier expansion of potential in the interstitial region. To ensure high resolution for MCA calculations, a dense k-mesh of 30 × 30 × 21 was used. The charge and energy convergence criteria were set to be 10^{-6} e and 10^{-6} Ry, respectively. The MCA and orbital moments are the relativistic effects and therefore, the spin-orbit coupling (SOC) was also incorporated in the calculations as a second-order perturbation to total energy. The SOC Hamiltonian, H_{SO} [24,25] yields the following change in ground state energies of the alloys:

Table 2
Calculated total and atom resolved spin magnetic moments (μ_s), orbital magnetic moments (μ_l), saturation magnetization (M_s) and MCA (K) of FeNi and FeNi:N uisng WIEN2k.

Compound	Direction	Magnetic Moments (μ_B)							M_s (T)	K (MJ/m^3)
FeNi			Fe		Ni		Total			0.43
	001	μ_s	2.701		0.645		3.272		1.66	
		μ_l	0.054		0.036		–		1.67 [30]	
	100	μ_s	2.702		0.645		3.272			
		μ_l	0.049		0.038		–			
	Expt.	μ_s	2.540 [28]		0.730 [29]				1.47 [8]	0.58–1.3 [7–9]
		μ_l	0.050 [28]		0.100 [29]					
FeNi:N(O_{Ni})			Fe_1	Fe_2	Fe_3	Ni	N	Total	1.53	0.95
	001	μ_s	2.740	2.895	2.037	0.579	0.059	3.226		
		μ_l	0.063	0.059	0.042	0.036	0.001	–		
	100	μ_s	2.741	2.895	2.038	0.580	0.060	3.229		
		μ_l	0.048	0.046	0.007	0.030	0.002	–		
FeNi:N(O_{Fe})			Fe	Ni_1	Ni_2	Ni_3	N	Total	1.46	0.63
	001	μ_s	2.394	0.346	0.861	0.847	−0.046	3.043		
		μ_l	0.047	0.024	0.054	0.053	0.004	–		
	100	μ_s	2.392	0.346	0.860	0.847	−0.045	3.041		
		μ_l	0.041	0.007	0.054	0.051	0.002	–		

Mizuguchi et al. [7], Poirier et al. [8], Paulevé et al. [9], Cable et al. [28], Kostugi et al. [29], Edström et al. [30].

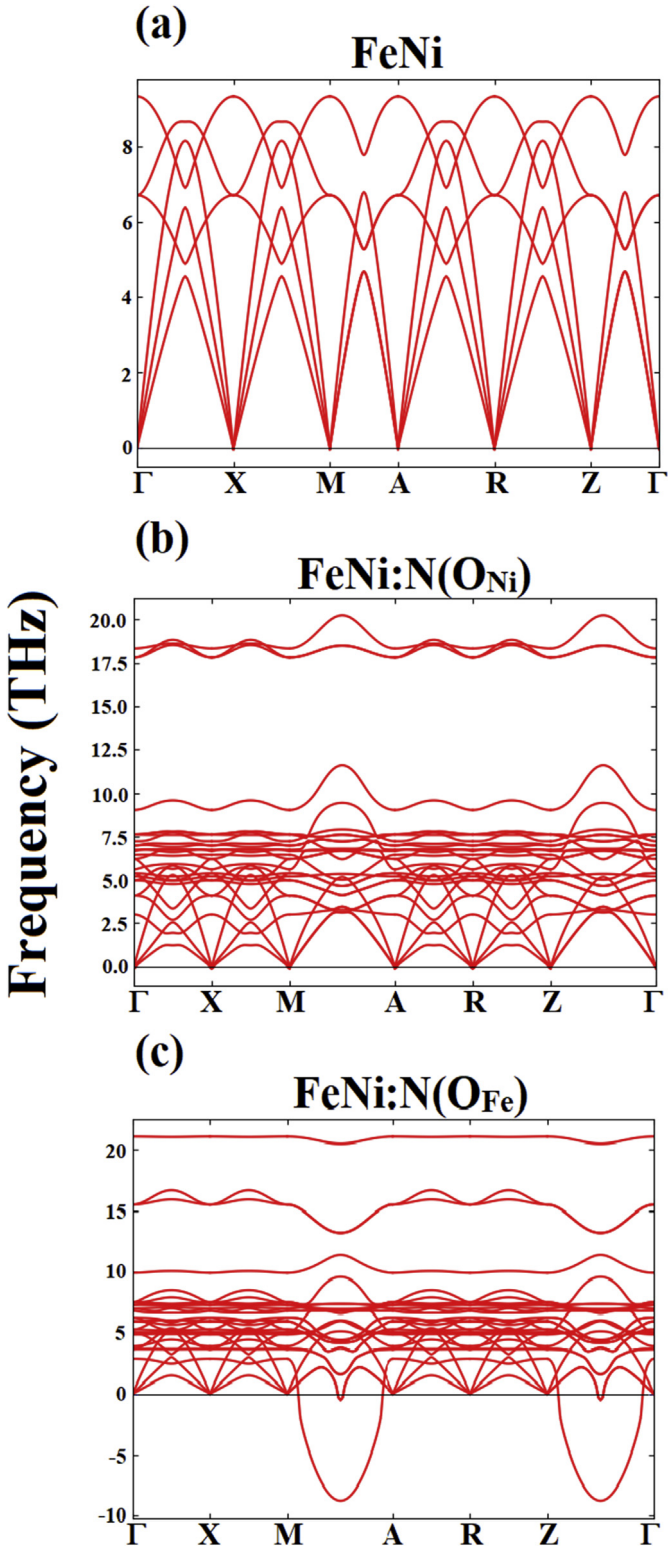

Fig. 2. Phonon dispersion curves for (a) FeNi (b) FeNi:N(O_{Ni}) and (c) FeNi:N(O_{Fe}).

$$\Delta E_{SO}^{(2)} = -\sum_{n,\sigma}^{occ.} \sum_{n',\sigma'}^{unocc.} \frac{|\langle n,\sigma|H_{SO}|n',\sigma'\rangle|^2}{E_{n',\sigma'}^{0} - E_{n,\sigma}^{0}} \quad (1)$$

where $n,\sigma>$ and $n',\sigma'>$ are unperturbed occupied (with band n, and spin σ) and unoccupied (with band n' and spin σ') energy states, respectively. $E_{n,\sigma}^{0}$ and $E_{n',\sigma'}^{0}$ represent the corresponding eigenvalues of these states. The MCA was calculated using the magnetic force theorem [26,27] with the formula:

$$MCA = E_{100} - E_{001} \quad (2)$$

where E_{100} and E_{001} are the summation of occupied band energy eigenvalues for magnetization vector oriented along [100] and [001] directions, respectively. The positive/negative value obtained from equation (2) indicates uniaxial/in-plane MCA.

3. Results and discussion

Fig. 1 shows the schematics of the 2 × 2 × 1 supercell of base material FeNi which is interstitially doped with a N-atom to simulate FeNi:N. Pristine FeNi in its 2 × 2 × 1 supercell clearly contains interstitial positions in Fe as well as Ni layers where a small foreign atom can easily be incorporated without distorting the $L1_0$-tetragonal crystal structure. After relaxation, it was observed that c/a ratio increases (Table 1) due to tetragonal distortion on interstitial N-doping in both layers.

Firstly, in order to check the structure stability, we have calculated the formation energy (E_{For}) of FeNi and FeNi:N (Table 1) by using the following formulae:

$$E_{For}^{FeNi} = E_{FeNi} - E_{Fe} - E_{Ni} \quad (3)$$

$$E_{For}^{FeNi:N} = (E_{FeNi:N} - 4E_{Fe} - 4E_{Ni} - 1/2\, E_{N2}) \Big/ 4 \quad (4)$$

where E_{FeNi}, $E_{FeNi:N}$, E_{Fe}, E_{Ni} and E_{N2} are the ground state energies of pristine FeNi, FeNi:N supercell, Fe, Ni and N_2 in their native states, respectively. These native states are bcc Fe, fcc Ni and N_2 molecule. The negative values of formation energies for all cases indicate the structural stability. We observed that the tetragonal distortion induced by N-doping promotes the formation of FeNi furthermore.

Further, as is well-known, the phonon dispersion spectra can be used to estimate dynamical structural stability. In this context, we have calculated the phonon dispersion for pristine and interstitially doped FeNi as shown in Fig. 2. It is found that the FeNi:N(O_{Fe}) phase is structurally unstable due to the imaginary phonon frequencies existing in phonon dispersion spectra, whereas the pristine and FeNi:N(O_{Ni}) phases have real frequencies and hence are dynamically stable structures.

For investigation of electronic properties, total and orbital projected density of states (DOS) of FeNi and FeNi:N are depicted in Fig. 3. The total DOS of FeNi is spin polarized while on addition of N, some states get accommodated near the Fermi level (E_F) in majority spin channel of FeNi:N which reduces its spin polarization.

In FeNi:N(O_{Ni}/O_{Fe}), due to asymmetry caused by interstitial N-impurity, all Fe/Ni atoms can be categorized as three non-equivalent atoms, denoted by (Fe_1, Fe_2 and Fe_3)/(Ni_1, Ni_2 and Ni_3). The DOS in the vicinity of E_F are due to the admixture of Fe_3-3d/Ni_3-3d and N-2p states.

The net magnetic moment can be computed by the difference of majority and minority spin states in the occupied region. The minority spin states are less filled in Fe ($3d^6$) as compared to Ni ($3d^8$) which results in larger spin magnetic moment for Fe (2.70 μ_B) than that of Ni (0.64 μ_B). The total spin magnetic moment of FeNi:N(O_{Ni}/

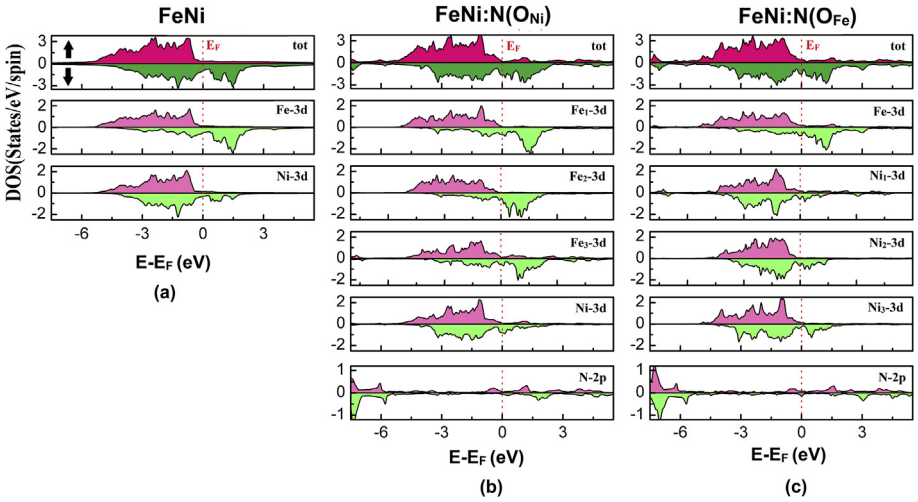

Fig. 3. Calculated total and orbital projected DOS of (a) FeNi (b) FeNi:N(O_{Ni}) and (c) FeNi:N(O_{Fe}) alloys. Fermi level (E_F) is shifted to 0 eV.

Table 3
Calculated lattice parameters (a,c), formation energy (E_{For}), MCA (K), saturation magnetization (M_s), coercivity (H_c) and maximum energy product ($(BH)_{max}$) of FeNi and FeNi:N(O_{Ni}) using WIEN2k.

Percentage	Supercell	a (Å)	c (Å)	c/a	E_{For} (eV)	K (MJ/m^3)	M_s (T)	H_c (MA/m)	$(BH)_{max}$ (kJ/m^3)
Pristine	–	2.531	3.579	1.414	−0.18	0.43	1.67	0.52	432
6.25	2 × 2 × 4	2.529	3.621	1.432	−0.93	0.52	1.62	0.64	519
12.5	2 × 2 × 2	2.536	3.662	1.444	−1.38	0.54	1.58	0.68	496
25.0	2 × 2 × 1	2.561	3.714	1.450	−2.35	0.95	1.53	1.24	465

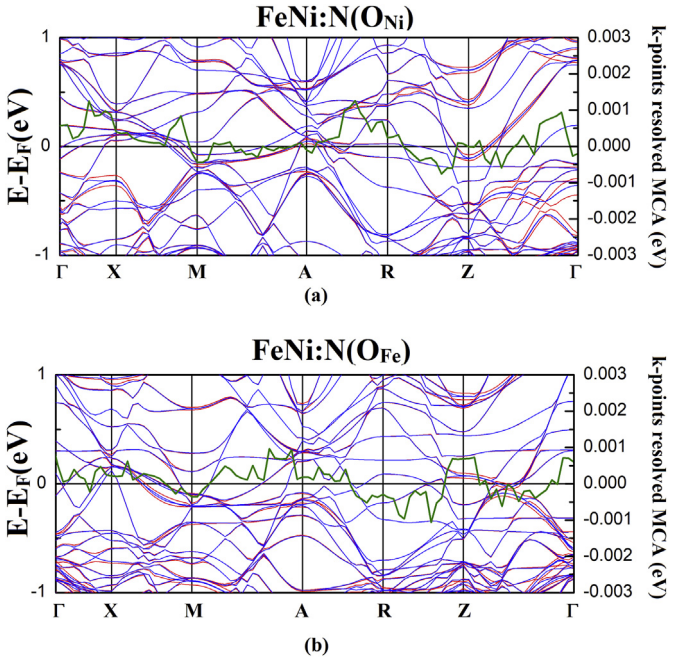

Fig. 4. Band structures including SOC with magnetization along [100] (blue lines) and [001] (red lines) directions along with the MCA contribution per k-point (green), obtained via the magnetic force theorem for majority spin states of (a) FeNi:N(O_{Ni}) (b) FeNi:N(O_{Fe}).

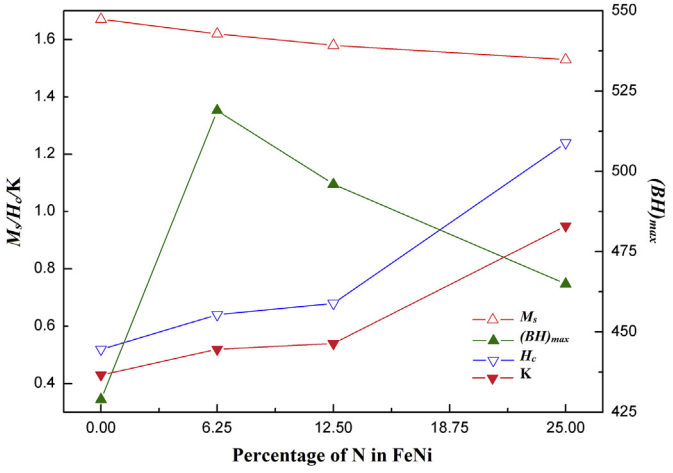

Fig. 5. Saturation magnetization (M_s), maximum energy product ($(BH)_{max}$), coercivity (H_c) and MCA (K) of FeNi:N(O_{Ni}) with different doping percentage of N.

O_{Fe}) decreases due to the hybridization of Fe_3-3d and Ni-3d/Fe-3d and Ni_3-3d with p-states of non-magnetic impurity atom (N-2p). This decrease is more in FeNi:N(O_{Fe}) due to antiparallel alignment of N-2p with Fe-3d and Ni-3d states. The calculated spin magnetic moments are isotropic for all the alloys. However, orbital magnetic moments are directional dependent and orbital moment anisotropy (OMA), defined by $\triangle\mu_l = \mu_l^{001} - \mu_l^{100}$, is found as 0.005 μ_B for Fe and −0.002 μ_B for Ni in pristine FeNi. This observation is in good agreement with Miuara et al. [11]. In case of FeNi:N(O_{Ni}), the observed OMA is 0.021/0.006/-0.001 μ_B for Fe/Ni/N and in FeNi:-N(O_{Fe}), this value is 0.006/0.006/0.002 μ_B. Hence, the overall sum of OMA increases in both cases.

The saturation magnetization (M_s) is defined as total magnetic moment per unit volume. However, in TM alloys, the orbital moments remain quenched due to crystal field effect. Therefore, total

magnetic moment is approximately equal to total spin magnetic moment. Thus, the M_s values for all cases have been calculated as total spin magnetic moment per unit volume which are listed in Table 2 along with the final values of MCA. The saturation magnetization of pristine FeNi is 1.66 T which is in close agreement to previously calculated theoretical value 1.67 T [30] and consistent with experimental results i.e. 1.47 T [8]. On interstitial N-doping, M_s decreases from 1.66 T to 1.53/1.46 T for FeNi:N(O_{Ni}/O_{Fe}) case. This decrease is larger in FeNi:N(O_{Fe}) due to decrease in Fe moment which exists in the plane containing non-magnetic N impurity. Further, Fe is anti-ferromagnetically coupled with N impurity in this situation. The calculated MCA of $L1_0$-FeNi is 0.43 MJ/m^3 which is comparable to 0.47 MJ/m^3 as calculated by Werwinski et al. [10] However, its experimentally measured value oscillates around 1 MJ/m^3 [6–10], depending on the synthesis technique used. On the addition of interstitial N-doping, the MCA increases to 0.95/0.63 MJ/m^3 for FeNi:N(O_{Ni}/O_{Fe}). This increase may be attributed to the tetragonal distortion i.e. increased c/a ratio. The similar observations were noticed by Miuara et al. [11] and Manchanda et al. [13] theoretically for pristine FeNi and FeNi:B case, respectively. On experimental front also, the increase in MCA with increasing c/a ratio was reported by Mizuguchi et al. [7] for $L1_0$-FeNi thin film. Further, the anisotropy energy per atom is directly proportional to OMA [31] i.e. larger OMA results large MCA. In FeNi:N, enhancement in OMA leads to large MCA. Moreover, in FeNi:N(O_{Ni}), orbital anisotropy is even larger that allows larger MCA (0.95 MJ/m^3) than that of FeNi:N(O_{Fe}) (0.63 MJ/m^3).

The structural stability and magnetic properties clarify that out of two FeNi:N alloys, FeNi:N(O_{Ni}) is more suitable candidate to act as permanent magnetic material. Therefore, we have checked the concentration variation of N in FeNi:N(O_{Ni}) only. From our calculations, we have found the obvious result (Table 3) i.e. the MCA increases on increasing the concentration of N-impurity at negligible cost of magnetization. This increase is clearly a consequence of tetragonal distortion induced due to the increased interstitial N-impurity. Moreover, increased tetragonal distortion furthermore promotes the structural stability of $L1_0$-FeNi. This is in agreement with the experimental result reported by Mizuguchi et al. [7].

In order to find the origin of the MCA, the electronic band structures with SOC along two magnetization directions [100] and [001] as well as MCA contribution at various k-points using the magnetic force theorem [26,27] are analyzed for majority spin state of FeNi:N in Fig. 4. As the MCA depends on the electronic structure in the vicinity of E_F (SOC constants of TMs are very low ~ 50–100 meV [32]), the band structures are plotted only near E_F. On analyzing band structures, it is found that difference in energies for both FeNi:N alloys is overall positive which leads to uniaxial anisotropy.

After knowing M_s and K, we can determine the intrinsic hard magnetic property, coercivity (H_c) and figure of merit i.e. maximum energy product $(BH)_{max}$. The coercivity (H_c) is anticipated by using empirical Kronmüller equation [3,33,34] after ignoring local demagnetizing factor.

$$H_c = \frac{2K}{\mu_0 M_s}\alpha \tag{5}$$

where α is the microstructure constant, in real systems, its value is less than one and depends on the shape and size of the grain, temperature, and other extrinsic quantities but here H_c has been estimated by setting $\alpha = 1$.

On the other hand, $(BH)_{max}$ is equal to twice of the maximum energy density which can be stored in a magnet (Table 3). The estimated value of $(BH)_{max}$ [35] is given by

$$(BH)_{max} = \begin{cases} \dfrac{\mu_0 M_s^2}{4} & H_c > M_s/2 \\ \dfrac{\mu_0 M_s H_c}{2} & H_c < M_s/2 \end{cases} \tag{6}$$

Fig. 5 shows the variation of magnetic response of FeNi:N(O_{Ni}) with different dopant concentrations. From this figure, we observe that the value of H_c and K increases with small suppression of M_s on increasing the N-concentration due to the increase in tetragonal distortion. In pristine FeNi, due to less coercivity, $(BH)_{max}$ is limited to 432 MJ/m^3. On introduction of N-impurity, firstly it increases and then decreases as the value of $(BH)_{max}$ becomes proportional to M_s^2 because of higher value of coercivity i.e. $H_c > M_s/2$.

4. Conclusion

In order to tune the magnetocrystalline anisotropy of $L1_0$-FeNi, the electronic and magnetic properties of FeNi and FeNi:N have been analyzed using full potential approach. The calculated results impart that interstitial N-doping induces tetragonal distortion that yields an increase in magnetocrystalline anisotropy at the cost of slight decrease in saturation magnetization due to hybridization of Fe/Ni-3d states with N-2p states. Further, our observations prove that the magnetocrystalline anisotropy and magnetization values for FeNi:N(O_{Ni}) case are more appropriate for permanent magnetic materials than that for FeNi:N(O_{Fe}). In the nutshell, FeNi:N(O_{Ni}) has the potential to act as auspicious material for RE free permanent magnets due to its large value of coerciviy as well as maximum energy product. We hope the predicted results will open a new avenue for testing FeNi with interstitial N-doping at experimental front also.

Declaration of competing interest

The authors declare that they have no known competing financial interests or personal relationships that could have appeared to influence the work reported in this paper.

CRediT authorship contribution statement

Priti Rani: Investigation, Software, Data curation, Validation, Visualization, Writing - original draft. **Manish K. Kashyap:** Conceptualization, Methodology, Supervision, Writing - review & editing, Formal analysis, Project administration, Funding acquisition. **Renu Singla:** Investigation, Visualization, Writing - original draft. **Jyoti Thakur:** Visualization, Writing - original draft, Writing - review & editing. **Ali H. Reshak:** Methodology, Writing - review & editing, Formal analysis.

Acknowledgement

The computation in this work was performed using Param Shavak supercomputing machine available at Department of Physics, Kurukshetra University, Kurukshetra (Haryana) and the National PARAM Supercomputing Facility (NPSF) of Centre for Development of Advanced Computing (C-DAC), Pune, India. P. Rani and M. K. Kashyap acknowledge Deparment of Science and Technology-Science and Engineering Research Board (DST-SERB) New Delhi, India for providing financial assistantship vide grant no. EMR/2016/007380.

Appendix A. Supplementary data

Supplementary data related to this article can be found at https://doi.org/10.1016/j.jallcom.2020.155325.

References

[1] K. Bourzac, The rare-earth crisis, Tech. Rev. 114 (2011) 58–63.
[2] D. Niarchos, G. Giannopoulos, M. Gjoka, C. Sarafidis, V. Psycharis, J. Rusz, A. Edstrom, O. Eriksson, P. Toson, J. Fidler, E. Anagnostopoulou, Toward rare-earth-free permanent magnets: a combinatorial approach exploiting the possibilities of modeling, shape anisotropy in elongated nanoparticles, and combinatorial thin-film approach, JOM 67 (2015) 1318–1328.
[3] R. Skomski, J.M.D. Coey, Magnetic anisotropy—how much is enough for a permanent magnet? Scripta Mater. 112 (2016) 3–8.
[4] D. Li, D. Pan, S. Li, Z.D. Zhang, Recent developments of rare-earth-free hard-magnetic materials, Science China Physics Mechanics & Astronomy 59 (2016) 617501.
[5] S. Hirosawa, M. Nishino, S. Miyashita, Perspectives for high-performance permanent magnets: applications, coercivity, and new materials, Adv. Nat. Sci. Nanosci. Nanotechnol. 8 (2017), 013002.
[6] L.H. Lewis, A. Mubarok, E. Poirier, N. Bordeaux, P. Manchanda, A. Kashyap, R. Skomski, J. Goldstein, F.E. Pinkerton, R.K. Mishra, R.C. Kubic Jr., Inspired by nature: investigating tetrataenite for permanent magnet applications, J. Phys.: Cond. Matr. 26 (2014), 064213.
[7] M. Mizuguchi, T. Kojima, M. Kotsugi, T. Koganezawa, K. Osaka, K. Takanashi, Artificial fabrication and order parameter estimation of $L1_0$-ordered FeNi thin film grown on a AuNi buffer layer, J. Magn. Soc. Japan 35 (2011) 370–373.
[8] E. Poirier, F.E. Pinkerton, R. Kubic, R.K. Mishra, N. Bordeaux, A. Mubarok, L.H. Lewis, J.I. Goldstein, R. Skomski, K. Barmak, Intrinsic magnetic properties of L_{10} FeNi obtained from meteorite NWA 6259, J. Appl. Phys. 117 (2015) 17E318.
[9] J. Paulevé, A. Chamberod, K. Krebs, A. Bourret, Magnetization curves of Fe-Ni (50-50) single crystals ordered by neutron irradiation with an applied magnetic field, J. Appl. Phys. 39 (1968) 989–990.
[10] M. Werwiński, W. Marciniak, Ab initio study of magnetocrystalline anisotropy, magnetostriction, and Fermi surface of $L1_0$ FeNi (tetrataenite), J. Phys. D Appl. Phys. 50 (2017) 495008.
[11] Y. Miura, S. Ozaki, Y. Kuwahara, M. Tsujikawa, K. Abe, M. Shirai, The origin of perpendicular magneto-crystalline anisotropy in $L1_0$-FeNi under tetragonal distortion, J. Phys.: Cond. Matr. 25 (2013) 106005.
[12] T. Kojima, M. Mizuguchi, T. Koganezawa, M. Ogiwara, M. Kotsugi, T. Ohtsuki, T.Y. Tashiro, K. Takanashi, Addition of Co to $L1_0$-ordered FeNi films: influences on magnetic properties and ordered structures, J. Phys. D Appl. Phys. 47 (2014) 425001.
[13] P. Manchanda, R. Skomski, N. Bordeaux, L.H. Lewis, A. Kashyap, Transition-metal and metalloid substitutions in $L1_0$-ordered FeNi, J. Appl. Phys. 115 (2014) 17A710.
[14] L.H. Lewis, K.B. Vaziri, Rare-earth-free Permanent Magnetic Materials Based on Fe-Ni, US 2017/0250024 A1, 2017.
[15] F. Takata, K. Ito, T. Suemasu, Fabrication of ordered Fe − Ni nitride film with equiatomic Fe/Ni ratio, Jpn. J. Appl. Phys. 5 (2018), 0–3.
[16] S. Goto, H. Kura, E. Watanabe, Y. Hayashi, H. Yanagihara, Y. Shimada, M. Mizuguchi, K. Takanashi, E. Kita, Synthesis of single-phase L10-FeNi magnet powder by nitrogen insertion and topotactic extraction, Sci. Rep. 7 (1) (2017) 1–7.
[17] S. Goto, H. Kura, H. Yanagihara, E. Kita, M. Tsujikawa, R. Sasaki, M. Shirai, Y. Kobayashi, T. Honda, K. Ono, Positive Weiss temperature in layered antiferromagnetic FeNiN for high-performance permanent magnets, ACS Appl. Nano Mater. 2 (11) (2019) 6909–6917.
[18] A.L. Wysocki, M.C. Nguyen, C.-Z. Wang, K.-M. Ho, Concentration-tuned tetragonal strain in alloys: application to magnetic anisotropy of $FeNi_{1-x}Co_x$, Phys. Rev. B 100 (2019) 104429.
[19] Priti Rani, Jyoti Thakur, Ankur Taya, Manish K. Kashyap, Magnetocrystalline anisotropy of Pt-doped $L1_0$-FeNi compound for clean energy applications, Vacuum 159 (2019) 186–190.
[20] R.S. Clarke, E.R.D. Scott, Tetrataenite-ordered FeNi, a new mineral in meteorites, Am. Mineral. 65 (1980) 624–630.
[21] G. Kresse, J. Furthmüller, Efficient iterative schemes for ab initio total-energy calculations using a plane-wave basis set, Phys. Rev. B 54 (1996) 11169.
[22] P. Blaha, K. Schwarz, G.K.H. Madsen, D. Kvasnicka, J. Luitz, R. Laskowski, F. Tran, L.D. Marks, WIEN2k an Augmented Plane Wave + Local Orbitals Program for Calculating Crystal Properties, Revised Edition WIEN2k, 19.1, Vienna University of Technology, Vienna, Austria, 2019, ISBN 3-9501031-1-2.
[23] J.P. Perdew, K. Burke, M. Ernzerhof, Generalized gradient approximation made simple, Phys. Rev. Lett. 77 (1996) 3865.
[24] P. Bruno, Tight-binding approach to the orbital magnetic moment and magnetocrystalline anisotropy of transition-metal monolayers, Phys. Rev. B 39 (1989) 865.
[25] G. Autes, C. Barreteau, D. Spanjaard, M.C. Desjonqueres, Magnetism of iron: from the bulk to the monatomic wire, J. Phys. Condens. Matter 18 (2006) 6785.
[26] R. Wu, A.J. Freeman, Spin−orbit induced magnetic phenomena in bulk metals and their surfaces and interfaces, J. Magn. Magn Mater. 200 (1999) 498–514.
[27] A.R. Mackintosh, O.K. Andersen, Electrons at the Fermi Surface, 1980, p. 2115.
[28] J.W. Cable, E.O. Wollan, Magnetic-moment distribution in NiFe and AuFe alloys, Phys. Rev. B 7 (1973) 2005.
[29] M. Kotsugi, M. Mizuguchi, S. Sekiya, M. Mizumaki, T. Kojima, T. Nakamura, H. Osawa, K. Kodama, T. Ohtsuki, T. Ohkochi, K. Takanashi, Origin of strong magnetic anisotropy in $L1_0$-FeNi probed by angular-dependent magnetic circular dichroism, J. Magn. Magn Mater. 326 (2013) 235–239.
[30] A. Edström, J. Chico, A. Jakobsson, A. Bergman, J. Rusz, Electronic structure and magnetic properties of $L1_0$ binary alloys, Phys. Rev. B 90 (1) (2014), 014402.
[31] R.L. Streever, Individual Co site contributions to the magnetic anisotropy of RCo_5 compounds and related structures, Phys. Rev. B 19 (1979) 2704.
[32] M. Vijayakumar, M.S. Gopinathan, Spin-orbit coupling constants of transition metal atoms and ions in density functional theory, J. Mol. Struct.: THEOCHEM 361 (1996) 15–19.
[33] H. Kronmüller, Theory of nucleation fields in inhomogeneous ferromagnets, Phys. Status Solidi 144 (1987) 385–396.
[34] I. Khan, H. Jisang, Tuning magnetocrystalline anisotropy of α''-Fe16N2 by interstitial impurity doping: a first principles study, J. Magn. Magn Mater. 433 (2017) 17–23.
[35] R. Skomski, J.M.D. Coey, Giant energy product in nanostructured two-phase magnets, Phys. Rev. B 48 (1993) 15812.